Impurity-Induced Magnetic Order in Low-Dimensional Spin-Gapped Materials

J. Bobroff,[1] N. Laflorencie,[1] L. K. Alexander,[1] A. V. Mahajan,[2] B. Koteswararao,[2] and P. Mendels[1]

[1]*Laboratoire de Physique des Solides, Université Paris-Sud, UMR-8502 CNRS, 91405 Orsay, France*
[2]*Department of Physics, Indian Institute of Technology Bombay, Mumbai 400076, India*

We have studied the effect of nonmagnetic Zn impurities in the coupled spin ladder $Bi(Cu_{1-x}Zn_x)_2PO_6$ using ^{31}P NMR, muon spin resonance (μSR), and quantum Monte Carlo simulations. Our results show that the impurities induce in their vicinity antiferromagnetic polarizations, extending over a few unit cells. At low temperature, these extended moments freeze in a process which is found universal among various other spin-gapped compounds: isolated ladders, Haldane, or spin-Peierls chains. This allows us to propose a simple common framework to explain the generic low-temperature impurity-induced freezings observed in low-dimensional spin-gapped materials.

The physics of low-dimension quantum antiferromagnets (AFM) is fascinating and surprising. Simple AFM spin chains or ladders display exotic low-temperature behavior such as spin liquids, spin gaps, magnetic orders, spin glasses, etc. The precise behavior depends on the value of the spin, the dimensionality of the material, the anisotropy, and the relative strengths and signs (possibly frustrating) of the magnetic couplings. Studying the effect of impurities is an efficient way to classify and reveal the quantum nature of these systems [1]. For example, the qualitatively different properties of half-integer and integer spin chains are evidenced in the strongly different impurity-induced effects in the two systems.

In AFM chains and ladders, nonmagnetic impurities induce paramagnetic clouds made of alternating moments in their vicinity, the shape and extension of which is directly linked to the type of electronic correlations involved in the ground state. At low enough temperatures, impurities may even lead to magnetic order or spin freezing, a sort of "order by disorder" phenomenon [2–8]. For example, a few percent of nonmagnetic Zn or Mg substituted at the Cu site of the spin-Peierls chain $CuGeO_3$ [3,7,8], the spin ladder $SrCu_2O_3$ [4,9], or at the Ni site of the Haldane chain $PbNi_2V_2O_8$ [5,10] leads to a collective freezing below a 3D ordering temperature T_g of a few K. The induced paramagnetic clouds can be viewed as effective localized moments extending over a finite region of typical size ξ around each impurity, with an exponentially decaying staggered magnetization $\langle S^z(r) \rangle \sim (-1)^r \times \exp(-r/\xi)$ [11–13]. A 3D effective interaction between them governs the freezing at low temperature. The frozen-state characteristics should then be specific to a given compound and geometry, explaining why no common picture has been given yet to understand the numerous experiments. As the effective interaction between impurities falls off exponentially with the distance r [14–17] as $J^{\text{eff}}(r) \sim J_0 \exp(-r/\xi)$, it has then been suggested that the relevant energy scale for the magnetic freezing is given by the *typical coupling*, i.e., the effective interaction occurring

at the average distance between impurities along the chains or the ladders $\langle r \rangle \simeq 1/x$ [7,15,18] where x is the impurity concentration. However, as pointed out in Ref. [19], realistic parameters would give exponentially small T_g, and a quantitative agreement with experimental values has been obtained using unrealistic enhanced lengths ξ [7,18].

To decide which actual process drives the freezing in impurity-doped spin-gapped materials, we have chosen to study the effect of impurities in a new spin-ladder material $BiCu_2PO_6$ (BCPO). In contrast with the archetypal ladder compound $SrCu_2O_3$ where ladders are almost isolated with a magnetic coupling $J_{\text{leg}} \simeq 2000$ K, BCPO has a non-negligible interladder coupling but a much smaller $J_{\text{leg}} \sim 100$ K [20]. We present here muon spin resonance (μSR) and NMR studies of the effects of nonmagnetic Zn impurities, together with quantum Monte Carlo (QMC) simulations. Above T_g, NMR enables one to measure the induced paramagnetic cloud near the impurities while μSR is an ideal probe of the frozen state, measuring both the freezing temperature T_g and the corresponding field distribution in the full volume of the sample. Our results compared to QMC simulations demonstrate that the extension of the induced clouds is only a few unit cells. This small extension, together with the 3D coupling J_{3D}, are the crucial parameters in the freezing process. We thus explain in a common framework the freezing temperatures observed in ladders and other low-dimension spin-gapped materials.

Synthesis and structural characterization of $Bi(Cu_{1-x}Zn_x)_2PO_6$ are presented elsewhere [20,21]. NMR measurements were performed using a 7 T home-made spectrometer with standard pulse techniques and Fourier transform recombinations. Magnetic susceptibility was measured in a SQUID magnetometer at $H = 0.1$ T. When Zn is substituted at Cu site, it is expected to release a free $S = 1/2$ spin. Macroscopic susceptibility indeed displays the signature of this free spin through a low-temperature Curie component proportional to Zn content. The fitted Curie constant corresponds to a total induced spin $S = 0.35$–0.45 per Zn slightly smaller than the ex-

pected $S = 1/2$ because of possible frustration effects
[21]. This total spin is not localized on a single site but
develops as an induced, extended, alternating cloud (AFM
cloud) along the ladder and in adjacent ones. This AFM
cloud reveals itself in the ^{31}P NMR spectrum through a
low-temperature broadening (Fig. 1) just as in isolated
ladders [9]. The spin-$\frac{1}{2}$ coupled ladders can be modeled by

$$\mathcal{H} = \sum_{\langle ij\rangle} J_{\text{leg}} \vec{S}_{i,j} \cdot \vec{S}_{i+1,j} + J_{\text{rung}} \vec{S}_{i,2j} \cdot \vec{S}_{i,2j+1}$$
$$+ J_{\perp} \vec{S}_{i,2j+1} \cdot \vec{S}_{i,2j+2}. \qquad (1)$$

As already studied in detail [22,23], this model displays a
gapped valence bond solid phase when the interladder
coupling $J_{\perp}$ is not too strong. For isotropic ladders ($J_{\text{rung}} =
J_{\text{leg}}$) this is the case when $J_{\perp} < J_{\perp}^c$ with $J_{\perp}^c/J =
0.314\,07(5)$ [22], and the correlation length diverges close
to the quantum critical point (QCP) $\xi \sim (J_{\perp}^c - J_{\perp})^{-\nu}$ with
$\nu = 0.709(6)$ [23]. Previous bulk studies on BCPO [20]
estimate $J_{\text{leg}} \simeq J_{\text{rung}} \sim 100$ K. Muffin-tin orbital calcula-
tions suggest the existence of an additional frustrating
coupling along the ladders [20]. We did not take this
possible frustration into account in our model Eq. (1) as
we just want to capture semiquantitative features of the
low-T physics. The experimental spin gap $\Delta \sim 35$ K
yields an interladder coupling $0.1 \leq J_{\perp}/J_{\text{leg}} \leq 0.2$, imply-
ing a small ξ. Using QMC simulations we have computed
the magnetization profile induced by a single impurity on a
32×32 lattice. Exponentially localized AFM profiles are
found with the 2D form

$$\langle S^z(\vec{r})\rangle \simeq S_0 \exp\left(-\frac{x}{\xi_x} - \frac{y}{\xi_y}\right)(-1)^{x+y} \qquad (2)$$

valid all over the gapped regime. The extensions ξ_x and ξ_y
at $T = 0$ are reported in Fig. 2(b) where one can clearly see
that they quantitatively follow the behavior of the pure
correlation length $\xi \sim J/\Delta$: the impurity-induced effect
reveals the intrinsic properties of the ladder, as in
Haldane chains [24,25] or high-T_c cuprates [26]. This
result contradicts analysis of Ref. [18] which argues that
the AFM cloud extension depends on the impurity content
and reaches values as large as 50 cell units at low concen-
trations. However, such conclusions were entirely based on
NMR experiments done at the very low $x = 0.1\%$ concen-
tration where the observed NMR broadenings are too small
to be reliable. All other data of Refs. [9,18] are fully
compatible with our own results and conclusions. As
shown in Fig. 2(a), the cloud extensions ξ_x and ξ_y increase
when the temperature is lowered but converge very rapidly
once the gap $\Delta \simeq 0.2$–$0.3J$ is reached. As a result, the
NMR broadening (Fig. 1) at low T follows the Curie law
due to S_0 only as expected (Fig. 1). QMC simulations
performed for $J_{\perp}/J = 0.1$ at $T = J/10$ with an external
field $H = J/10$ over 32×32 sites with $x = 2\%$ of non-
magnetic impurities are averaged over 10^2 disordered
samples to obtain the distribution of local fields seen by
each phosphorus plotted in the right-hand panel of Fig. 1.
The simulated broadening found without any adjustable
parameter is remarkably similar to the experimental ones,
albeit possible frustration is not considered.

In order to probe whether these impurity-induced AFM
clouds of only a few unit cell extension lead to a freezing in
BCPO, we performed a μSR study on the same Zn sub-
stituted BCPO samples at the PSI (GPS) facility. Pressed
disks of randomly oriented powders were used. Muons
which carry a spin $1/2$ are implanted in the samples and
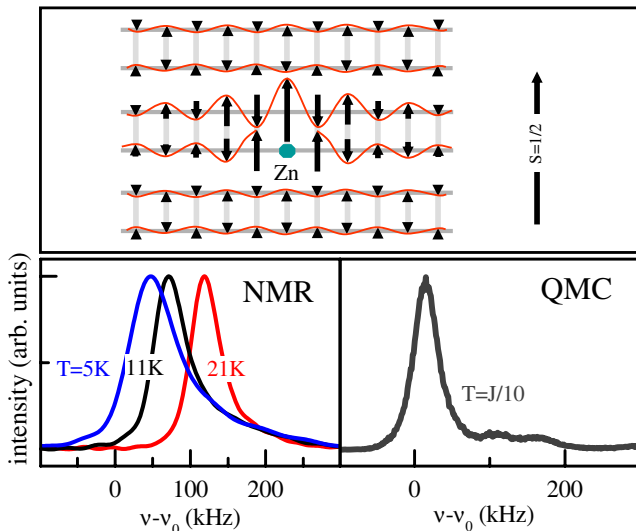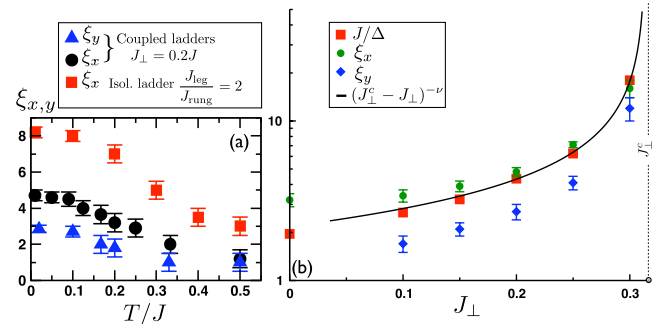precess around the local magnetic field. This precession is

FIG. 1 (color online).   Lower panel. Left: ^{31}P NMR spectra for
BCPO, Zn 2% at $H = 7$ T. Right: QMC results for the coupled
ladders model Eq. (1) at $T = J/10$ with an applied field $H =
J/10$, using $J_{\text{leg}} = J_{\text{rung}} = J$, $J_{\perp}/J = 0.1$, $x = 2\%$. The corre-
sponding Zn induced magnetic pattern in the ladders is displayed
in the top panel, with a $S = 1/2$ arrow indicating the scale.

FIG. 2 (color online).   QMC results for the AFM cloud exten-
sions and the correlation length of model (1). (a) T dependence
of the induced extensions ξ_x and ξ_y for coupled and isolated
ladders ($SrCu_2O_3$ has $J_{\text{leg}}/J_{\text{rung}} = 2$). (b) $T = 0$ results for the
inverse gap $J/\Delta \sim \xi$ and the extensions ξ_x, ξ_y vs $J_{\perp}$. The black
line is the pure correlation length $\xi \sim (J_{\perp}^c - J_{\perp})^{-\nu}$ (see text).
The small error bars come from the uncertainty in the 3 parame-
ter fit of QMC data to Eq. (2).

measured through the detection of the asymmetry of the positron emission due to the muon decay. In the absence of an external magnetic field ("zero field setup"), above T_g, only the tiny nuclear spin dipolar fields are experienced by the muons. This results in a Gaussian field distribution and a very slowly decaying "Kubo-Toyabe" polarization as displayed in Fig. 3 at $T = 10$ K. When the electronic spins start to freeze below T_g, their randomly oriented static moments result in a much larger field distribution and a much faster decaying asymmetry as shown in Fig. 3 at $T = 1.6$ K. We checked that this depolarization is of static origin below T_g by applying a large longitudinal field and finding the expected asymmetry decoupling. Since no marked oscillations are observed, the corresponding field distribution is not that of a simple commensurate magnetic ordering. However, due to the lack of a dip in the asymmetry, it is probably not completely random as in a spin glass, but more likely in an intermediate situation with AFM clusters, as discussed in Ref. [27]. To get an estimate of the field distribution, we used the same phenomenological exponential field distribution as in Ref. [27], which fits well the data as shown in Fig. 3. The resulting static field distribution develops as a mere order parameter which allows one to determine T_g. Whatever the impurity nature or concentration, the transition temperature is proportional to the field distribution even for very large impurity concentrations.

The SrCu$_2$O$_3$ ladder shows similar time dependence for the muon polarization as displayed in Fig. 3 [27]. Both the static field distribution and T_g [4] are found 1.7 times larger than in BCPO. This 1.7 ratio is unexpectedly about 1 order of magnitude smaller than the ratio between the ladder couplings. Other low-dimensional spin gap systems such as Haldane chains or spin-Peierls chains also display
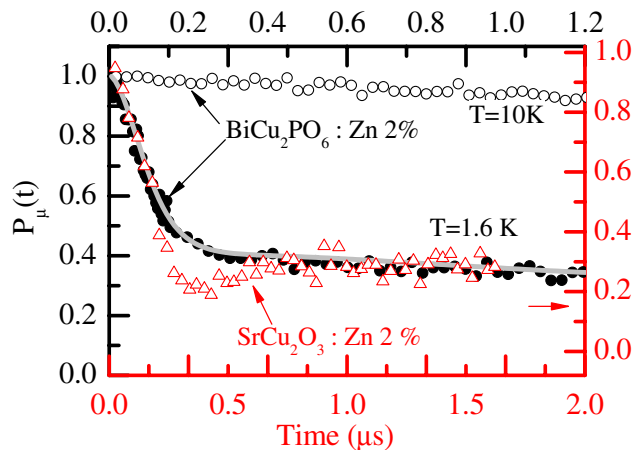
very similar T_g despite their different geometries and gap values (Fig. 4). The dependence on impurity content also shows a strikingly generic behavior, with a similar departure from a linear behavior at about 2%–3% for all compounds as demonstrated in the right-hand panel of Fig. 4. Magnetic impurities in these materials also lead to similar T_g and similar concentration dependence as shown in Fig. 4.

Despite several theoretical investigations devoted to understanding the origin of the impurity-induced 3D ordering in low-dimensional gapped systems [15,17,19,28,29], no common framework has emerged so far which explains this generic T_g behavior. The collective freezing of the effective moments (having a 3D extension $\sim \xi_x \xi_y \xi_z$ at $T > T_g$) is actually controlled by the exponentially decaying 3D coupling of the general form

$$|J_{3D}^{\text{eff}}(\vec{r})| \simeq J_{3D} \exp\left(-\frac{x}{\xi_x} - \frac{y}{\xi_y} - \frac{z}{\xi_z}\right), \quad (3)$$

expected to occur for the wide class of spin-gapped materials [14–17,30,31]. Couplings in the three directions are necessary to allow finite-T ordering due to the Mermin-Wagner theorem, and J_{3D} is the weakest of these couplings. The typical coupling $J_{\text{typ}} = |J_{3D}^{\text{eff}}(\langle r \rangle)|$, taken at the average distance $\langle r \rangle$ between impurities, is much too small to explain the actual 3D freezing temperatures [19] because it does not take into account the rare but crucial situations where r is small. On the contrary, the average coupling J_{av} taken over all possible $J_{3D}^{\text{eff}}(\vec{r})$ does account for the broad distribution of effective interactions and is just given by

$$J_{\text{av}} = \langle |J_{3D}^{\text{eff}}(\vec{r})| \rangle \simeq J_{3D} \frac{x V_\xi}{1 + x V_\xi}, \quad (4)$$

FIG. 3 (color online). Muon polarization for BCPO above and below T_g (black circles) on upper and left axis is compared to a similar experiment made in SrCu$_2$O$_3$ (bottom axis being rescaled, right axis is slightly shifted because of a different background) from Ref. [27]. Gray line is a fit to Eq. (3) of Ref. [27] as explained in the text.
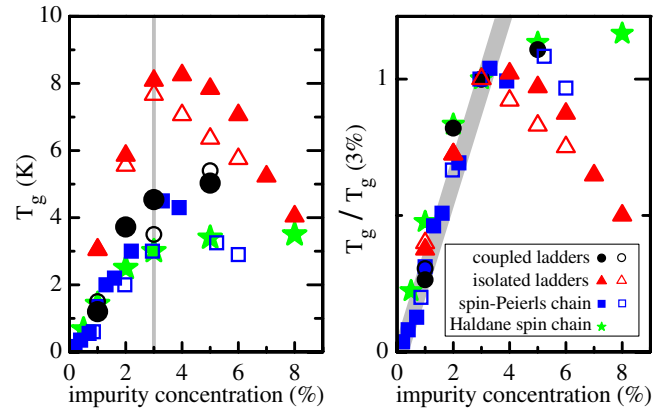

FIG. 4 (color online). Left: Transition temperatures versus impurity concentration for various low-dimensional spin-gapped systems: coupled ladders Bi(Cu$_{1-x}$(Zn or Ni)$_x$)$_2$PO$_6$ from this study, isolated ladder Sr(Cu$_{1-x}$(Zn or Ni)$_x$)$_2$O$_3$ [4,18], Haldane chain Pb(Ni$_{1-x}$Mg$_x$)$_2$V$_2$O$_8$ [36], spin-Peierls chains Cu$_{1-x}$(Zn or Ni)$_x$GeO$_3$ [8]. Full symbols and open symbols correspond, respectively, to nonmagnetic and magnetic impurities. Right: Same data where T_g is rescaled by its value at $x = 3\%$.

where $V_\xi \sim \xi_x \xi_y \xi_z$ is the magnetic volume occupied by each induced moment. We propose that this average coupling governs the ordering, i.e., $T_g \simeq J_{av}$. Indeed, this model accounts well for the fact that all T_g are similar in magnitude, because both J_{3D} and V_ξ are roughly of the same order of magnitude among the different systems. Precise values for J_{3D} are not known since they are at most a few percent of the dominant coupling. However, rough estimates give a few K for $CuGeO_3$ [32] and $PbNi_2V_2O_8$ [5]. For $SrCu_2O_3$ a theoretical calculation [28] based on an isotropic ladder model found $J_{3D} \sim 20$ K. Even though the order of magnitude is correct, the actual J_{3D} is probably smaller because of the anisotropy $J_{leg} = J_{rung} = 2$ [33]. Regarding BCPO, based on our analysis we can confidently predict a 3D coupling ~ 5 K. Turning now to the magnetic volumes V_ξ of the induced moments, they are similar at low temperature, typically ~ 30 sites, despite the geometric differences between systems. For instance, Zn in the almost isolated anisotropic ladders $Sr(Cu_{1-x}Zn_x)_2O_3$ induces a cigarlike pattern, with $V_\xi \simeq 2 \times 8 \times 2 \simeq 32$. In the coupled ladders $Bi(Cu_{1-x}Zn_x)_2PO_6$ with $J_\perp/J \simeq 0.15$, Zn induces a pancakelike volume $V_\xi \simeq 2 \times 3.9 \times 2 \times 2.1 \simeq 33$. This is because all these spin-gapped materials are far enough from a QCP so that the various ξ remain a few unit cells and do not diverge (Fig. 2), whereas a totally different physics would be observed at criticality [34].

Such an analysis allows one to understand the concentration dependence of T_g as well. At small x, the average volume between impurities $\langle r \rangle^3 \sim x^{-1}$ is large compared to the magnetic volume V_ξ, and Eq. (4) implies a linear behavior of $T_g \simeq J_{av}$ with x. At larger x, extended moments get close enough to percolate, and the critical temperature is not linear with x anymore. This should occur at $x \sim 1/V_\xi \simeq 1/30 \simeq 3\%$. This prediction of a linear increase of T_g below $x \simeq 3\%$ and a deviation above is exactly what is observed in Fig. 4 (see also supplementary material [35] in which QMC simulations are presented).

In summary, the framework we propose to explain the impurity-induced freezings in various systems is based on the fact that the impurity induces an extended magnetic moment, the volume of which is similar in all systems because all lie far from the QCP. These induced moments interact through a 3D interaction which is not very sensitive to the geometry or the gap nature. This holds for magnetic impurities as well. It will be interesting to understand if this universal picture survives when a quantum critical point is approached.

[1] H. Alloul, J. Bobroff, M. Gabay, and P. Hirschfeld, Rev. Mod. Phys. **81**, 45 (2009).
[2] E. F. Shender and S. A. Kivelson, Phys. Rev. Lett. **66**, 2384 (1991).
[3] M. Hase *et al.*, Phys. Rev. Lett. **71**, 4059 (1993).
[4] M. Azuma *et al.*, Phys. Rev. B **55**, R8658 (1997).
[5] Y. Uchiyama *et al.*, Phys. Rev. Lett. **83**, 632 (1999).
[6] A. Oosawa, T. Ono, and H. Tanaka, Phys. Rev. B **66**, 020405 (2002).
[7] K. Manabe *et al.*, Phys. Rev. B **58**, R575 (1998).
[8] B. Grenier *et al.*, Phys. Rev. B **58**, 8202 (1998); V. Simonet *et al.*, Eur. Phys. J. B **53**, 155 (2006).
[9] N. Fujiwara *et al.*, Phys. Rev. Lett. **80**, 604 (1998).
[10] T. Masuda *et al.*, Phys. Rev. B **66**, 174416 (2002).
[11] S. R. White, R. M. Noack, and D. J. Scalapino, Phys. Rev. Lett. **73**, 886 (1994).
[12] G. B. Martins *et al.*, Phys. Rev. Lett. **78**, 3563 (1997).
[13] A. W. Sandvik, E. Dagotto, and D. J. Scalapino, Phys. Rev. B **56**, 11 701 (1997).
[14] M. Sigrist and A. Furusaki, J. Phys. Soc. Jpn. **65**, 2385 (1996).
[15] M. Imada and Y. Iino, J. Phys. Soc. Jpn. **66**, 568 (1997).
[16] C. Yasuda *et al.*, Phys. Rev. B **64**, 092405 (2001).
[17] N. Laflorencie and D. Poilblanc, Phys. Rev. Lett. **90**, 157202 (2003); N. Laflorencie, D. Poilblanc, and A. W. Sandvik, Phys. Rev. B **69**, 212412 (2004).
[18] S. Ohsugi *et al.*, Phys. Rev. B **60**, 4181 (1999).
[19] M. Fabrizio, R. Mélin, and J. Souletie, Eur. Phys. J. B **10**, 607 (1999); R. Mélin, Eur. Phys. J. B **18**, 263 (2000).
[20] B. Koteswararao *et al.*, Phys. Rev. B **76**, 052402 (2007); O. Mentr *et al.*, J. Am. Chem. Soc. **128**, 10 857 (2006).
[21] L. Alexander *et al.* (to be published); B. Koteswararao *et al.* (to be published).
[22] M. Matsumoto *et al.*, Phys. Rev. B **65**, 014407 (2001).
[23] S. Wenzel, L. Bogacz, and W. Janke, Phys. Rev. Lett. **101**, 127202 (2008).
[24] F. Tedoldi, R. Santachiara, and M. Horvatić, Phys. Rev. Lett. **83**, 412 (1999).
[25] J. Das *et al.*, Phys. Rev. B **69**, 144404 (2004).
[26] S. Ouazi *et al.*, Phys. Rev. B **70**, 104515 (2004).
[27] M. I. Larkin *et al.*, Phys. Rev. Lett. **85**, 1982 (2000).
[28] T. Miyazaki *et al.*, J. Phys. Soc. Jpn. **66**, 2580 (1997).
[29] M. Greven and R. J. Birgeneau, Phys. Rev. Lett. **81**, 1945 (1998).
[30] S. Wessel *et al.*, Phys. Rev. Lett. **86**, 1086 (2001).
[31] H. Weber and M. Vojta, Eur. Phys. J. B **53**, 185 (2006).
[32] L.-P. Regnault *et al.*, Phys. Rev. B **53**, 5579 (1996).
[33] D. C. Johnston, Phys. Rev. B **54**, 13 009 (1996).
[34] S. Sachdev, C. Buragohain, and M. Vojta, Science **286**, 2479 (1999); K. H. Höglund, A. W. Sandvik, and S. Sachdev, Phys. Rev. Lett. **98**, 087203 (2007).
[35] See EPAPS Document No. E-PRLTAO-103-027932 for QMC simulations. For more information on EPAPS, see http://www.aip.org/pubservs/epaps.html.
[36] M. Imai *et al.*, arXiv:cond-mat/0402595v1.